Mineralogical Magazine, June 2010, Vol. 74(3), pp. 553–565

Thermal behaviour of libethenite from room temperature up to dehydration

M. ZEMA[1,2,*], S. C. TARANTINO[1,2] AND A. M. CALLEGARI[1]

[1] Dipartimento di Scienze della Terra, Università degli Studi di Pavia, via Ferrata 1, I-27100 Pavia, Italy
[2] CNR-IGG, Sezione di Pavia, via Ferrata 1, I-27100 Pavia, Italy

[*Received 22 April 2010; Accepted 25 June 2010*]

ABSTRACT

The structural modifications with temperature of libethenite, $Cu_2(PO_4)(OH)$, were determined by single-crystal X-ray diffraction up to dehydration and consequent decomposition of the crystal under investigation. In the temperature range 25−475ºC, libethenite shows positive and linear expansion. The axial thermal expansion coefficients, determined over this temperature range, are: $\alpha_a = 6.6(1)\cdot10^{-6}$ K^{-1}, $\alpha_b = 1.21(2)\cdot10^{-5}$ K^{-1}, $\alpha_c = 9.0(2)\cdot10^{-6}$ K^{-1}, $\alpha_V = 2.78(3)\cdot10^{-5}$ K^{-1}. Axial expansion is then anisotropic with α_a:α_b:α_c = 1:1.83:1.33.

Structure refinements of X-ray diffraction data collected at different temperatures allowed us to characterize the mechanisms by which the libethenite structure accommodates variations in temperature. Increasing temperature induces expansion of both Cu polyhedra and no significant variation of the PO_4 tetrahedron, which acts as a rigid unit. Cu(1) octahedra expand mostly as a consequence of the increase of the axial bonds, and become more distorted. Starting from T = 500ºC, precursor signs of incoming dehydration are visible: two adjacent OH groups approach each other and cause dramatic changes in the whole structure. Concomitantly, the libethenite crystal begins to deteriorate and, at T = 600ºC, broad and weak diffraction effects of polycrystalline material are observed.

KEYWORDS: libethenite, thermal expansion, single-crystal X-ray diffraction.

Introduction

LIBETHENITE, $Cu_2(PO_4)(OH)$, is a member of the olivenite group, and occurs as a secondary mineral in the oxidized zones of copper ore deposits. Members of the group generally crystallize in the orthorhombic space group *Pnnm* (Huminicki and Hawthorne, 2002; Mills *et al*., 2010, and references therein), with a structure derived from that of andalusite, although olivenite has recently been confirmed as monoclinic $P2_1/n$ (Li *et al*., 2008).

The libethenite crystal structure was solved by Heritsch (1940) and subsequently detailed by means of single crystal X-ray diffraction (SC-XRD) on natural (Cordsen, 1978; Keller *et al*., 1979) and synthetic (Belik *et al*., 2007) samples. In the libethenite crystal structure (Fig. 1), Cu ions are located in two independent crystallographic sites, named Cu(1) and Cu(2), having octahedral and trigonal bipyramidal geometries, respectively. Cu(1) octahedra form straight chains along *c* by edge-sharing (alternately O2−O2 and O4−O4), the chains are cross-linked by isolated PO_4 tetrahedra *via* corner-sharing, thus forming an open network with channels extending in the *c* direction. Cu(2) trigonal bipyramids share the O3−O3 edge and form dimers which lie in these channels. Dimers are connected to octahedra chains and to PO_4 tetrahedra by sharing corners. Each hydroxyl group (O4 site) is shared by two octahedral and one trigonal bipyramidal Cu ions. Hydrogen atoms lie on a mirror plane and form

* E-mail: michele.zema@unipv.it
DOI: 10.1180/minmag.2010.074.3.553

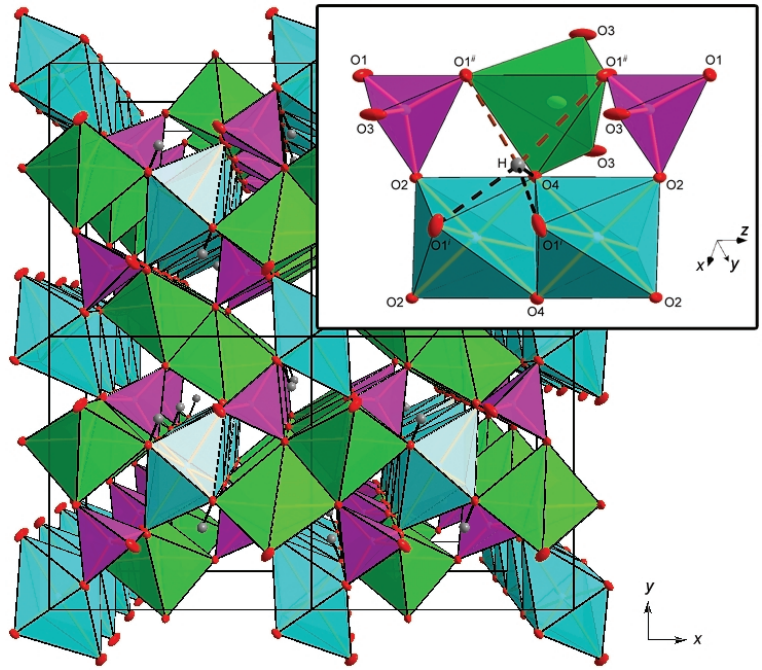

FIG. 1. Perspective view of crystal structure of libethenite plotted along *c*. Thermal ellipsoids are plotted at 50% probability level. Light blue: Cu(1) octahedra forming straight chains along *c*; green: Cu(2) trigonal bipyramids forming isolated dimers occupying channels running along *c*; purple: P tetrahedra. Hydrogen atoms are reported in grey. Inset: detail of the crystal structure highlighting the possible H-bonding network. Symmetry codes refer to hydrogen position: (i) $-x$, $-y$, $\pm z$; (ii) $\frac{1}{2}-x$, $\frac{1}{2}+y$, $\pm(\frac{1}{2}-z)$.

bifurcated hydrogen bonds with O1 oxygen atoms. The presence of the Jahn-Teller active Cu^{2+} ions induces distortion in the geometrical arrangements of the polyhedra. Differential thermal analysis (DTA) and thermogravimetric analysis (TG) analyses indicated that libethenite is stable up to ~650ºC (Xiao *et al*., 2001), when dehydration occurs, and libethenite is expected to transform into $Cu_4(PO_4)_2O$, which is known to crystallize either in a triclinic (Brunel-Laügt *et al*., 1978) or in an orthorhombic (Schwunck *et al*., 1998) polymorph.

Libethenite is known for some peculiar properties and applications. For example, even showing small surface area, it has been found to have a high catalytic activity in oxidation processes and, in particular, to be one of the best catalysts for the hydroxylation of phenol by H_2O_2 (Xiao *et al*., 2001). Cu-containing minerals, due their peculiar crystal structures and magnetic ion sub-lattices, often show interesting magnetic properties. In particular, synthetic libethenite has been found to be a spin-gap system with weak spin-exchange Cu−Cu interactions both within the Cu(2) dimers and within the Cu(1) chains, but strong interactions between dimers and chains (Belik *et al*., 2007).

Here, we present a structural investigation performed by *in situ* high-temperature single crystal X-ray diffraction (SC-XRD) of a natural libethenite in the range 25−575ºC, i.e. up to decomposition of the crystal consequent to starting of the dehydration process.

Experimental

Sample

A natural libethenite from Banska Bystrica region (Slovakia) was used in the present study. The chemical composition of this sample is close to the nominal one, as revealed by SEM/EDS analyses performed on four different crystals; only minor Al and Fe impurities (<1%) are in fact present. The SC-XRD study was carried out on a

transparent, light green crystal having dimensions 0.36 mm × 0.35 mm × 0.08 mm and showing sharp and narrow diffraction profiles.

SC-XRD at room temperature

Single-crystal diffraction data were collected at room temperature by means of a Bruker-AXS APEX diffractometer equipped with a CCD detector. Data collection was carried out with operating conditions 50 kV and 30 mA and graphite-monochromatized Mo-*K*α radiation (λ = 0.71073 Å). The Bruker *SMART* system of programs was used for preliminary crystal-lattice determination and X-ray data collection. A total of 3360 frames (resolution: 512 × 512 pixels) were collected with four different goniometer settings using the ω-scan mode (scan width: 0.2ºω; exposure time: 5 s/frame; detector–sample distance: 40 mm). Completeness of measured data was achieved up to 38.2ºθ. The Bruker program *SAINT*+ was used for the data reduction, including intensity integration, background and Lorentz-polarization corrections. Final unit-cell parameters were obtained by the Bruker *GLOBAL* least-squares orientation matrix refinement procedure, based on the positions of all measured reflections. The semi-empirical absorption correction of Blessing (1995), based on the determination of transmission factors for equivalent reflections, was applied using the Bruker program *SADABS* (Sheldrick, 2003). Details on room-temperature data collection by the CCD diffractometer are reported in Table 1.

SC-XRD at high temperature

In situ high-temperature single-crystal diffraction investigations were carried out using a Philips PW1100 four-circle diffractometer with point-counter detector. Operating conditions were 55 kV and 30 mA and graphite-monochromatized Mo-*K*α radiation (λ = 0.71073 Å). Horizontal and vertical apertures were 2.0º and 1.5º, respectively. A home-made U-shaped microfurnace with a K-type thermocouple was used. Temperature was previously calibrated by known melting points, and reported temperatures are precise to within ±5º. The selected crystal was inserted into a sealed quartz capillary (0.5 mm Ø) and kept in position by means of quartz wool. Unit-cell parameters were measured from room temperature up to 575ºC in steps of 25ºC. At each working temperature, the orientation matrix was updated by centering 24 reflections selected in the range ~7.7−15.6ºθ, and accurate lattice parameters (reported in Table 2) were derived from a least-squares procedure based on the Philips LAT routine over 43 to 54 d^* spacings, each measured considering all the reflections in the range 3º< θ < 26º. At the highest working temperatures (T > 550ºC), due to lowering of diffracted intensities, only 16−18 d^* spacings could be measured.

Complete datasets of diffracted intensities were collected at T = 25, 100, 200, 300, 400, 450, 500, and 550ºC using the same operating conditions as reported above. The equivalent reflections *hkl* and $hk\bar{l}$ were measured in the 2−26.5ºθ range by the ω/2θ scan mode (2.0ºθ scan width; 0.1ºθ/s scan speed). The microfurnace itself limits the angular region to these values. Three standard reflections were collected every 200 measured reflections. The XRD intensities were obtained by measuring step-scan profiles and analysing them by the Lehman and Larsen (1974) σ_I/I method, as modified by Blessing *et al*. (1974). Intensities were corrected for absorption using the semi-empirical ψ-scan method of North *et al*. (1968). Relevant parameters on data collections

TABLE 1. Details of data collection by the CCD diffractometer and structure refinement of libethenite at room temperature.

a (Å)	8.0614(2)
b (Å)	8.3972(2)
c (Å)	5.8870(1)
V (Å^3)	398.51(2)
$Trans_{min}/Trans_{max}$	0.45
θ max	38.2
Reflections measured	7399
Unique reflections	1164
Average I/σ_I	63.29
R_{int} (%)	2.45
Reflections with $I > 2\sigma$	1117
R_1[a] (%)	2.17
R_{all}[a] (%)	2.30
wR_2 (%)	5.22
GooF[b]	1.094
max, min Δρ (e·Å^{-3})	2.00, −1.61

[a] $R = \Sigma||F_o| - |F_c||/\Sigma|F_o|$ (R_1 is calculated on reflections with $I > 2\sigma_I$)

[b] GooF = S = $[\Sigma\ [w(F_o^2 - F_c^2)^2]/(n - p)]^{0.5}$, where n is the number of reflections and p is the total number of parameters refined.

TABLE 2. Unit-cell parameters of libethenite at different temperatures.

T (ºC)	*a* (Å)		*b* (Å)		*c* (Å)		*V* (Å^3)	
25	8.0600	(5)	8.3949	(3)	5.8858	(4)	398.24	(4)
50	8.0603	(5)	8.3962	(5)	5.8846	(5)	398.25	(5)
75	8.0615	(4)	8.3998	(4)	5.8863	(4)	398.59	(4)
100	8.0626	(5)	8.4031	(6)	5.8882	(5)	398.93	(5)
125	8.0645	(6)	8.4051	(4)	5.8894	(4)	399.20	(5)
150	8.0664	(6)	8.4074	(4)	5.8916	(5)	399.55	(5)
175	8.0664	(5)	8.4108	(5)	5.8915	(4)	399.70	(4)
200	8.0687	(6)	8.4134	(6)	5.8929	(6)	400.04	(5)
200	8.0680	(6)	8.4124	(5)	5.8931	(6)	399.97	(5)
225	8.0700	(6)	8.4155	(6)	5.8942	(5)	400.30	(6)
250	8.0708	(6)	8.4181	(7)	5.8957	(6)	400.56	(6)
275	8.0727	(6)	8.4204	(6)	5.8969	(7)	400.85	(6)
300	8.0740	(7)	8.4240	(6)	5.8982	(7)	401.17	(7)
325	8.0761	(6)	8.4257	(7)	5.9000	(6)	401.48	(6)
350	8.0777	(7)	8.4275	(7)	5.9010	(6)	401.71	(6)
375	8.0778	(7)	8.4320	(6)	5.9036	(6)	402.10	(6)
400	8.0796	(8)	8.4350	(8)	5.9034	(7)	402.33	(7)
400*	8.0793	(7)	8.4330	(8)	5.9045	(6)	402.29	(7)
425	8.0811	(7)	8.4366	(9)	5.9049	(7)	402.58	(7)
450	8.0813	(11)	8.4358	(12)	5.9068	(10)	402.68	(11)
475	8.0818	(12)	8.4383	(19)	5.9085	(9)	402.94	(13)
500	8.0838	(17)	8.4442	(21)	5.9072	(14)	403.23	(16)
525	8.0932	(14)	8.4429	(15)	5.9087	(16)	403.74	(15)
550	8.0996	(41)	8.4467	(52)	5.9063	(23)	404.08	(36)
575	8.1120	(41)	8.4800	(31)	5.8933	(12)	405.40	(27)

Standard deviations are given in parentheses
* Measured after data collection and used for structure refinement

performed at high temperature are reported in Table 3. Some reflections, representative of different classes, were also scanned periodically (ω/2θ scan mode; 2.0ºθ scan width; 0.1ºθ/s scan speed) to check for the crystallinity of the sample.

Structure refinements

All structure refinements were carried out in space group *Pnnm* by full-matrix least-squares using *SHELXL*-97 (Sheldrick, 1998). Equivalent reflections were averaged, and the resulting internal agreement factors R_{int} are reported in Table 1 for CCD data and in Table 3 for the HT datasets. The atomic scattering curves for neutral atoms were taken from the *International Tables for X-ray Crystallography* (Ibers and Hamilton, 1974). For all structure refinements, structure factors were weighted according to $w = 1/[\sigma^2(F_o^2 + 2F_c^2) + (AP)^2 + BP]$, where $P = (F_o^2 + 2F_c^2)/3$, and A and B were chosen for every crystal to produce a flat analysis of variance in terms of F_c^2 as suggested by the program. An extinction parameter x was refined to correct the structure factors according to the equation: $F_o = F_c\ k\ [1 + 0.001x\ F_c^2\lambda^3/\sin 2\theta]^{-1/4}$ (where k is the overall scale factor).

Structure refinement from data collected at room temperature on the CCD diffractometer was performed starting from the model of Cordsen (1978) with origin in 2*a* (0,0,0). All non-hydrogen atoms were refined anisotropically. The hydrogen position was located in the difference-Fourier map and inserted in the refinement with isotropic displacement parameter. All parameters were refined simultaneously. Possible hydrogen bonds resulting from refined positions are highlighted in the inset of Fig. 1. A residual peak at 0.59 Å from Cu(2) was observed in the final difference-Fourier map. Inclusion of such a peak in the refinement did not help in improving the agreement factor. Such a peak is not evident when structure refinement is limited to 30ºθ. Details on structure

TABLE 3. Details on HT data collections and structure refinements for libethenite.

T (ºC)	25	100	200	300	400	450	500	550
Reflections measured	838	842	844	844	846	847	843	845
Unique reflections	461	463	464	464	465	466	466	467
Average I/σ_I	32.79	33.33	30.77	24.94	30.67	27.40	10.22	5.17
R_{int} (%)	3.38	3.19	3.50	4.58	3.47	4.05	12.87	26.89
Reflections with $I > 2\sigma_I$	394	383	382	375	370	375	352	330
R_1[a] (%)	2.35	2.35	2.36	2.51	2.64	3.00	4.45	6.88
R_{all} (%)	3.22	3.38	3.54	3.72	4.18	4.53	6.80	9.44
wR_2 (%)	6.45	6.51	5.10	5.88	5.16	7.23	11.08	15.06
GooF[b]	1.213	1.144	1.150	1.112	1.114	1.118	1.132	1.122
max $\Delta\rho$ (e·Å^{-3})	0.55	0.56	0.53	0.58	0.73	0.72	1.16	1.27
min $\Delta\rho$ (e·Å^{-3})	−0.55	−0.58	−0.74	−0.83	−0.93	−1.11	−1.17	−1.14

[a] $R = \Sigma \, ||F_{o|} - |F_c||/\Sigma \, |F_{o|}$ (R_1 is calculated on reflections with $I > \sigma_I$)
[b] GOF = S = $[\Sigma \, [w(F_o^2 - F_c^2)^2]/(n - p)]^{0.5}$, where n is the number of reflections and p is the total number of parameters refined

refinement from room-temperature data collected by the CCD diffractometer are given in Table 1.

Structure refinements of data collected by the diffractometer with a point-counter detector were carried out starting from the model refined from CCD data at room temperature, and for the high-temperature datasets using the model obtained at the immediately lower temperature. Despite the lower resolution of these datasets, the hydrogen position was still evident in the difference-Fourier maps up to 450ºC. In these cases, hydrogen was added in the structural model, with coordinates fixed to position found in difference-Fourier maps and isotropic displacement parameters proportional ($\times 3$, on the basis of RT high-resolution refinement) to that of the neighbouring O4 atom, and not refined. At greater temperatures it was maintained fixed at the position found at 450ºC. All parameters were refined simultaneously. No significant peaks were present in the final difference-Fourier maps.

The values of the conventional agreement indices, R_1 and R_{all}, as well as the goodness of fit (S) are reported in Table 1 for the CCD data at room temperature and in Table 3 for the HT datasets. Fractional coordinates and anisotropic displacement parameters, U_{ij}, are reported in Table 4 for all the datasets, whereas interatomic distances and selected geometrical parameters are reported in Table 5. Observed and calculated structure factors have been deposited with the Principal Editor of *Mineralogical Magazine* and are available from www.minersoc.org/pages/e_journals/dep-mat.html.

Results and discussion

The unit-cell parameters and volume of libethenite are plotted as a function of temperature in Fig. 2. In the range 25−475ºC, libethenite shows positive and linear expansion. The thermal expansion coefficients, determined over this temperature range by least-squares regression analysis, are: $\alpha_a = 6.6(1)\cdot10^{-6}$ K^{-1}, $\alpha_b = 1.21(2)\cdot10^{-5}$ K^{-1}, $\alpha_c = 9.0(2)\cdot10^{-6}$ K^{-1}, $\alpha_V = 2.78(3)\cdot10^{-5}$ K^{-1}. Axial expansion is anisotropic with α_a:α_b:α_c = 1:1.83:1.33. Quantitative estimation of structure-controlled thermal expansion anisotropy was derived using the formalism of Schneider and Eberhard (1990): $A = (|\alpha(b) - \alpha(c)| + |\alpha(b) - \alpha(a)| + |\alpha(c) - \alpha(a)|) \times 10^{-6}$, which yielded a value of 1.10 K^{-1}. Anisotropy of axial thermal expansion in the range 25−450ºC can be rationalized in terms of polyhedra connectivity. Expansion is limited by edge-sharing Cu(2) dimers along a and by edge-sharing Cu(1) octahedra chains along c; on the other hand, connections of polyhedra along b, the direction of maximum expansion, is guaranteed by corner-sharing. Starting from T = 500ºC, dramatic deviations from linearity, i.e. abrupt increase of a and b lattice parameters and decrease of c, indicate incipient dehydration. Concomitantly, the crystal deteriorates significantly, diffraction

TABLE 4. Amount of fractional coordinates and anisotropic displacement parameters U_{ij} ($\times 10^{-4}$) for libethenite.

T (ºC)	25*	25	100	200	300	400	450	500	550
Site Cu(1), Wyckoff position 4*e* (0,0,*z*)									
z/*c*	0.24927(4)	0.24917(12)	0.24932(12)	0.24927(13)	0.24923(13)	0.24946(15)	0.24946(16)	0.24974(25)	0.25024(43)
U_{11}	102(1)	125(4)	145(4)	178(3)	213(4)	244(4)	251(5)	237(7)	250(11)
U_{22}	148(1)	157(3)	187(4)	228(4)	272(4)	309(4)	343(6)	411(8)	466(14)
U_{33}	63(1)	65(4)	80(4)	94(4)	106(4)	124(4)	152(4)	161(7)	130(14)
U_{12}	-57(1)	-58(2)	-65(3)	-86(3)	-106(3)	-116(4)	-130(5)	–138(6)	–135(10)
U_{eq}	104(1)	116(2)	138(2)	167(2)	197(2)	226(2)	249(3)	270(4)	282(7)
Site Cu(2), Wyckoff position 4*g* (*x*,*y*,0)									
x/*a*	0.13828(3)	0.13821(7)	0.13830(7)	0.13846(8)	0.13854(9)	0.13871(9)	0.13884(11)	0.13879(15)	0.13929(25)
y/*b*	0.62477(3)	0.62469(8)	0.62471(9)	0.62461(10)	0.62468(11)	0.62457(12)	0.62453(15)	0.62432(22)	0.62317(33)
U_{11}	55(1)	74(4)	86(4)	100(3)	124(4)	141(4)	142(5)	116(7)	122(11)
U_{22}	137(1)	151(3)	177(4)	220(4)	268(4)	301(5)	342(6)	414(9)	496(16)
U_{33}	202(1)	211(4)	244(5)	291(5)	328(5)	379(6)	427(7)	441(10)	457(20)
U_{12}	7(1)	9(3)	12(3)	12(3)	17(3)	21(4)	22(5)	25(7)	30(10)
U_{eq}	131(1)	145(2)	169(2)	203(2)	240(3)	274(3)	304(3)	324(5)	359(9)
Site P, Wyckoff position 4*g* (*x*,*y*,0)									
x/*a*	0.23276(6)	0.23282(15)	0.23281(15)	0.23217(16)	0.23168(17)	0.23123(18)	0.23070(21)	0.23105(32)	0.23094(53)
y/*b*	0.24825(6)	0.24824(15)	0.24816(16)	0.24825(16)	0.24844(17)	0.24850(18)	0.24859(22)	0.24817(30)	0.24872(49)
U_{11}	53(2)	82(6)	83(6)	102(6)	121(7)	130(7)	127(8)	110(11)	155(18)
U_{22}	77(2)	83(6)	106(6)	110(6)	136(7)	144(7)	163(9)	207(12)	226(19)
U_{33}	76(2)	83(7)	92(8)	106(8)	117(8)	130(8)	157(9)	154(13)	156(25)
U_{12}	−10(1)	−8(5)	−13(5)	−17(5)	−24(5)	−21(6)	−28(8)	−16(10)	−24(17)
U_{eq}	69(1)	83(3)	94(4)	106(4)	124(4)	135(4)	149(5)	157(6)	179(11)
Site O1, Wyckoff position 8*h* (*x*,*y*,*z*)									
x/*a*	0.34078(16)	0.34099(31)	0.34061(33)	0.33968(34)	0.33932(36)	0.33821(38)	0.33817(47)	0.33957(67)	0.3386(11)
y/*b*	0.26088(15)	0.26107(30)	0.26099(32)	0.26073(33)	0.26109(35)	0.26107(36)	0.26087(48)	0.26063(66)	0.2611(11)
z/*c*	0.21143(20)	0.21181(50)	0.21133(55)	0.21088(58)	0.21107(60)	0.21091(59)	0.21085(66)	0.2103(11)	0.2106(21)
U_{11}	180(5)	168(14)	210(15)	247(15)	273(16)	335(17)	340(21)	305(28)	330(45)
U_{22}	186(5)	179(11)	203(12)	253(14)	293(14)	321(16)	351(21)	455(29)	587(50)
U_{33}	117(4)	123(14)	152(18)	182(18)	198(18)	200(19)	203(19)	223(30)	257(60)
U_{23}	53(4)	39(12)	53(13)	59(14)	72(14)	66(15)	73(19)	80(28)	67(59)
U_{13}	−65(4)	−42(12)	−71(12)	−86(14)	−80(15)	−102(17)	−86(18)	−120(29)	−84(55)
U_{12}	−94(4)	−93(11)	−112(12)	−127(12)	−140(13)	−163(14)	−169(19)	−162(26)	−157(42)
U_{eq}	161(3)	156(8)	188(9)	227(9)	255(9)	285(10)	298(12)	328(17)	391(30)

Site O2, Wyckoff position 4*g* (*x*,*y*,0)									
x/a	0.13322(18)	0.13339(44)	0.13311(45)	0.13246(50)	0.13198(55)	0.13128(55)	0.13133(69)	0.12910(98)	0.1289(15)
y/b	0.08837(18)	0.08799(37)	0.08864(41)	0.08876(42)	0.08952(44)	0.08942(46)	0.09084(60)	0.09193(77)	0.0912(12)
U_{11}	98(5)	117(17)	124(18)	162(18)	233(21)	230(21)	271(26)	236(37)	264(61)
U_{22}	96(5)	89(17)	137(19)	171(20)	182(21)	198(24)	231(29)	242(38)	194(53)
U_{33}	77(5)	66(18)	80(20)	83(20)	91(20)	123(22)	146(24)	201(38)	145(66)
U_{12}	−40(4)	−24(12)	−32(14)	−76(16)	−99(16)	−81(19)	−99(24)	−74(32)	−95(49)
U_{eq}	90(3)	91(10)	114(11)	139(11)	169(12)	184(13)	216(15)	226(22)	201(35)
Site O3, Wyckoff position 4*g* (*x*,*y*,0)									
x/a	0.10232(21)	0.10221(47)	0.10219(48)	0.10219(45)	0.10184(49)	0.10211(49)	0.10251(62)	0.10274(86)	0.1016(13)
y/b	0.38394(20)	0.38475(44)	0.38441(45)	0.38397(50)	0.38480(51)	0.38357(56)	0.38440(69)	0.3843(10)	0.3821(15)
U_{11}	64(5)	87(17)	105(17)	96(18)	130(19)	153(21)	149(24)	75(30)	70(47)
U_{22}	86(6)	104(17)	71(16)	129(19)	137(20)	163(22)	170(26)	230(36)	310(61)
U_{33}	457(12)	457(30)	542(33)	579(36)	657(39)	675(42)	747(46)	966(95)	965(168)
U_{12}	3(5)	−7(14)	−13(15)	−14(17)	7(18)	−4(20)	−14(24)	9(33)	6(49)
U_{eq}	203(5)	216(13)	240(13)	268(14)	308(16)	330(17)	355(19)	424(34)	448(60)
Site O4, Wyckoff position 4*g* (*x*,*y*,0)									
x/a	0.37667(18)	0.37577(42)	0.37628(44)	0.37675(45)	0.37703(48)	0.37650(49)	0.37780(61)	0.37851(93)	0.3792(16)
y/b	0.60256(18)	0.60174(39)	0.60206(41)	0.60248(43)	0.60259(44)	0.60228(49)	0.60240(64)	0.60325(89)	0.6019(14)
U_{11}	64(5)	83(16)	100(16)	112(16)	135(18)	148(18)	165(22)	159(33)	261(62)
U_{22}	97(5)	92(17)	131(18)	140(19)	171(20)	177(22)	241(29)	327(41)	347(66)
U_{33}	105(5)	124(20)	110(20)	160(22)	148(22)	206(25)	226(26)	278(44)	313(86)
U_{12}	3(4)	−11(12)	20(14)	11(15)	7(16)	26(18)	18(23)	88(34)	46(57)
U_{eq}	89(3)	100(10)	114(10)	137(11)	152(11)	177(12)	211(15)	254(22)	307(41)
Site H, Wyckoff position 4*g* (*x*,*y*,0)									
x/a	0.417(7)	0.41680	0.43050	0.41510	0.41000	0.41830	0.42540	not refined	not refined
y/b	0.699(6)	0.69450	0.71980	0.70290	0.70490	0.69510	0.69083	not refined	not refined
U_{iso}	424(137)	300	341	411	455	531	632	–	–

Standard deviations are given in parentheses
*CCD data

TABLE 5. Bond distances (Å) and selected geometrical parameters.

T (ºC)	25*	25	100	200	300	400	450	500	550
Cu(1) octahedron									
Cu(1)−O1 (×2)	2.394(1)	2.391(2)	2.396(3)	2.404(3)	2.406(3)	2.413(3)	2.414(4)	2.413(5)	2.415(8)
Cu(1)−O2 (×2)	1.964(1)	1.963(2)	1.965(2)	1.964(3)	1.966(3)	1.966(3)	1.971(4)	1.967(5)	1.967(7)
Cu(1)−O4 (×2)	1.977(1)	1.978(2)	1.977(2)	1.979(3)	1.980(3)	1.982(3)	1.978(4)	1.977(5)	1.968(8)
<Cu(1)−O>	2.112(1)	2.111(2)	2.113(2)	2.116(3)	2.117(3)	2.120(3)	2.121(4)	2.119(5)	2.117(8)
Volume (Å^3)	12.19	12.18	12.20	12.25	12.27	12.32	12.33	12.27	12.23
OAV	40.63	39.22	39.99	41.09	41.27	40.67	41.85	46.01	44.93
OQE	1.0293	1.0287	1.0291	1.0301	1.0302	1.0305	1.0309	1.0324	1.0326
O4−O4 edge	2.631(2)	2.632(5)	2.631(5)	2.632(5)	2.633(5)	2.638(6)	2.624(7)	2.626(11)	2.607(18)
O2−O2 edge	2.611(2)	2.609(5)	2.613(5)	2.607(6)	2.611(6)	2.603(6)	2.618(8)	2.601(11)	2.595(16)
O2−O4 edge	2.9470(1)	2.9461(3)	2.9472(3)	2.9497(4)	2.9513(4)	2.9549(4)	2.9559(6)	2.9563(8)	2.955(13)
O2−Cu(1)−O4 (º)	96.79(4)	96.8(1)	96.8(1)	96.9(1)	96.8(1)	96.9(1)	96.9(1)	97.1(2)	97.4(3)
Cu(2) trigonal bipyramid									
Cu(2)−O1 (×2)	2.054(1)	2.053(2)	2.057(3)	2.060(3)	2.063(3)	2.067(3)	2.068(4)	2.070(6)	2.076(11)
Cu(2)−O3	2.043(2)	2.035(3)	2.040(4)	2.045(4)	2.042(4)	2.054(5)	2.047(6)	2.048(8)	2.059(11)
Cu(2)−O3^i	1.941(2)	1.939(3)	1.941(4)	1.943(4)	1.943(4)	1.947(4)	1.952(5)	1.954(7)	1.952(10)
Cu(2)−O4	1.931(2)	1.925(3)	1.928(4)	1.932(4)	1.935(4)	1.930(4)	1.940(5)	1.946(8)	1.951(13)
<Cu(2)−O>	2.005(2)	2.001(3)	2.004(3)	2.008(4)	2.009(4)	2.013(4)	2.015(5)	2.017(7)	2.023(11)
Volume (Å^3)	6.95	6.91	6.95	6.99	6.99	7.04	7.05	7.08	7.14
O3−O3 edge	2.554(2)	2.542(5)	2.547(5)	2.555(6)	2.544(6)	2.565(6)	2.559(8)	2.565(11)	2.584(16)
P tetrahedron									
P−O1 (×2)	1.523(1)	1.525(2)	1.522(3)	1.519(3)	1.522(3)	1.520(3)	1.522(4)	1.524(6)	1.523(11)
P−O2	1.564(2)	1.566(3)	1.563(4)	1.564(4)	1.562(4)	1.566(4)	1.554(5)	1.556(7)	1.566(10)
P−O3	1.551(2)	1.556(3)	1.556(4)	1.550(4)	1.555(4)	1.545(5)	1.545(6)	1.548(8)	1.538(12)
<P−O>	1.540(2)	1.543(3)	1.541(3)	1.538(4)	1.540(4)	1.537(4)	1.536(5)	1.538(7)	1.538(11)
Volume (Å^3)	1.87	1.88	1.87	1.87	1.87	1.86	1.86	1.86	1.86
TAV	2.46	2.20	2.52	2.37	2.32	2.45	2.13	3.86	4.76
TQE	1.0007	1.0007	1.0008	1.0007	1.0007	1.0008	1.0006	1.0010	1.0013
Cation−cation distances									
Cu(1)...Cu(1)	2.9349(3)	2.933(1)	2.936(1)	2.938(1)	2.939(1)	2.946(1)	2.947(1)	2.9510(2)	2.956(4)
Cu(2)...Cu(2)	3.0596(4)	3.057(1)	3.060(1)	3.064(1)	3.069(1)	3.072(1)	3.074(1)	3.073(1)	3.069(4)

Possible hydrogen bonds O4–H...O1								
O4–H (Å)	0.876(51)	0.846(3)	1.082(3)	0.900(4)	0.902(4)	0.852(4)	0.839(5)	0.831(8)	0.839(12)
O4...O1^{i} (Å)	2.838(2)	2.845(4)	2.843(4)	2.847(4)	2.848(5)	2.862(5)	2.855(6)	2.838(9)	2.848(15)
H...O1^{i} (Å)	2.340(45)	2.346(3)	2.232(3)	2.356(3)	2.393(3)	2.357(3)	2.317(4)	2.306(6)	2.317(10)
O4–H–O1^{i} (º)	116.22(3)	118.14(6)	113.60(7)	114.25(7)	111.34(7)	118.33(7)	122.29(10)	122.26(14)	121.66(22)
O4...O1^{ii} (Å)	2.780(2)	2.778(4)	2.780(4)	2.779(4)	2.781(4)	2.778(5)	2.784(6)	2.793(8)	2.800(14)
H...O1^{ii} (Å)	2.733(42)	2.740(3)	2.791(3)	2.714(3)	2.679(3)	2.742(3)	2.793(4)	2.804(6)	2.801(10)
O4–H–O1^{ii} (º)	83.88(3)	83.76(5)	78.28(6)	84.71(6)	86.97(6)	83.50(6)	80.71(8)	80.73(11)	81.33(18)

Standard deviations are given in parentheses. Symmetry codes as in Fig. 1: (i) $-x,-y,\pm z$; (ii) $\frac{1}{2}-x,\frac{1}{2}+y,\pm(\frac{1}{2}-z)$.
Polyhedral angular variance (TAV, OAV) and quadratic elongation (TQE, OQE) as defined by Robinson *et al.* (1971).
* CCD data

FIG. 2. Variation of unit-cell parameters and volume with temperature for libethenite. Linear regressions calculated in the range 25–475ºC are reported as solid lines.

profiles become broad and intensities weaken. In Fig. 3, diffraction profiles of the 440 reflection measured at different temperatures are reported as an example. At T = 600ºC, only weak and broad diffraction effects, not indexable by a unique phase, are observed.

Structure refinements of room- and high-temperature diffraction data allowed analysis of the thermal structural modifications. Hereafter, modifications occurring in the range 25−450ºC, i.e. due to thermal expansion of hydrated libethenite, will be discussed separately from variations occurring at T > 500ºC, forerunner of incipient dehydration.

Polyhedral mean bond lengths are reported in Fig. 4. Increasing temperature in the range 25−450ºC induces expansion of both Cu polyhedra and no significant variation of the PO_4 tetrahedron, which acts as a rigid unit. This is clearly evident also when the P−O bond distances corrected for thermal motion are taken into account. It is well known from the literature that the interatomic distances measured by XRD are typically underestimated and appropriate corrections, which imply the use of accurate estimates of anisotropic displacement parameters (ADPs), should be applied. To perform the correction for thermal motion in a general case, it is necessary to know, in addition to the ADPs, the correlation tensors between the displacement of the bonded atoms, which cannot be deduced directly from Bragg diffraction measurements, but in principle can be obtained by lattice-dynamical calculations. Without assuming any specific model for vibration (e.g. rigid body, riding or uncorrelated motion, etc.), bond distances cannot be corrected for thermal motion; nonetheless an estimate of the possible errors, i.e. an upper and a lower limit for the corrected interatomic distances, can be obtained (Busing and Levy, 1964; Johnson,

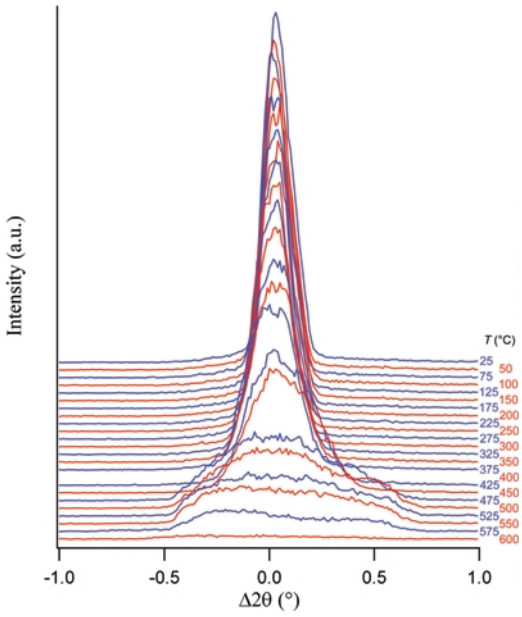

FIG. 3. Diffraction profiles of reflection 440 at different temperatures.

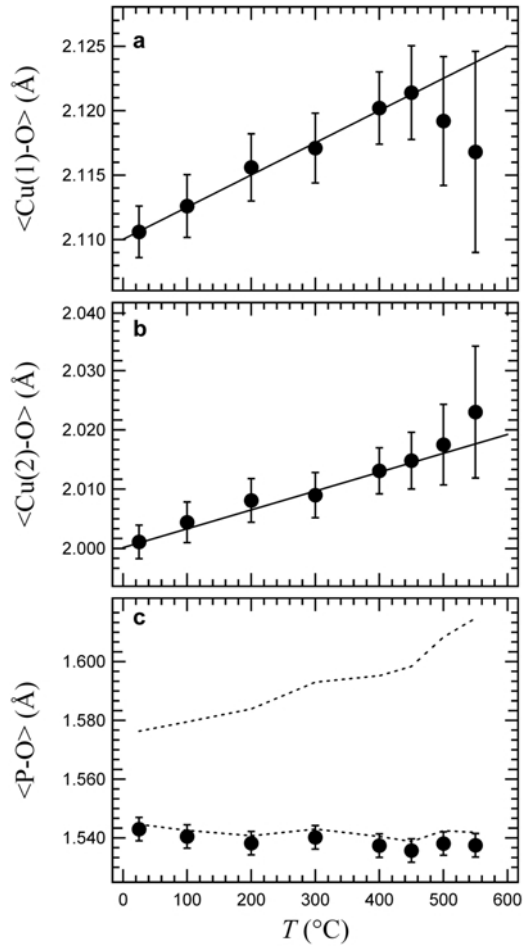

FIG. 4. Mean bond lengths as a function of temperature. (*a*) Cu(1)−O; (*b*) Cu(2)−O; (c) P−O. Circles: uncorrected bond distances. Solid lines: linear regressions calculated in the range 25−450ºC. Dashed lines: upper and lower limits for the corrected P−O interatomic distances.

1970*a*,*b*; Scheringer, 1972). Such values are reported in Fig. 4*c* for <P−O> distances and confirm that only slight expansion of the tetrahedron is allowed. Distortion of this polyhedron does not vary significantly in the 25−450ºC temperature range, as indicated by the tetrahedral distortion parameters (Robinson *et al*., 1971) reported in Fig. 5.

Copper ions show severely distorted coordination due to the Jahn-Teller effect. In particular, Cu(1) octahedra show extremely elongated axial bonds which, in turn, cause oxygen atoms in the [Cu(1)O_4] basal plane to lie too far away from Cu(2) ions to participate in their coordination, which remains 5-fold. Displacement parameters refined for the Cu(1) ion show a preferential direction of elongation which corresponds to the O1−Cu(1)−O1 axial vector [Cu(1) thermal ellipsoid axes ratio R_{max}/R_{min} ~3], and this is maintained across the whole temperature range investigated (see data in Table 4). With increasing temperature, Cu(1) octahedra expand (see Fig. 4*a*) mostly as a consequence of the increase of Cu(1)−O1 axial bonds [the four basal Cu(1)−O distances do not vary significantly in extent; see data in Table 5], and hence become more distorted, as indicated by the octahedral distortion parameters (Robinson *et al*., 1971) reported in Fig. 6. Modifications occurring on the octahedron basal plane are of less extent and induce little extension of the chain with increasing temperature. The Cu(1)...Cu(1) distance in fact increases with temperature (Fig. 7*a*), as a consequence of the slight and linear increase of the unshared O2−O4 edge (Fig. 8*a*) and of the O2−Cu(1)−O4 angle (see data in Table 5 and inset in Fig. 1). The O2−O2 and O4−O4 shared edges do not vary significantly in this temperature range (Fig. 8*b*,*c*). With regard to the Cu(2) dimers, a linear increase of the Cu(2)...Cu(2) distance (Fig. 7*b*) as well as an increase of the O3−O3 common edge (Fig. 8*d*) are observed.

Starting from T = 500ºC, precursor signs of incoming dehydration are detected. The process should involve loss of H_2O, and not OH^- or H_2 alone, according to $2(OH) \rightarrow H_2O(\uparrow) + O_r$

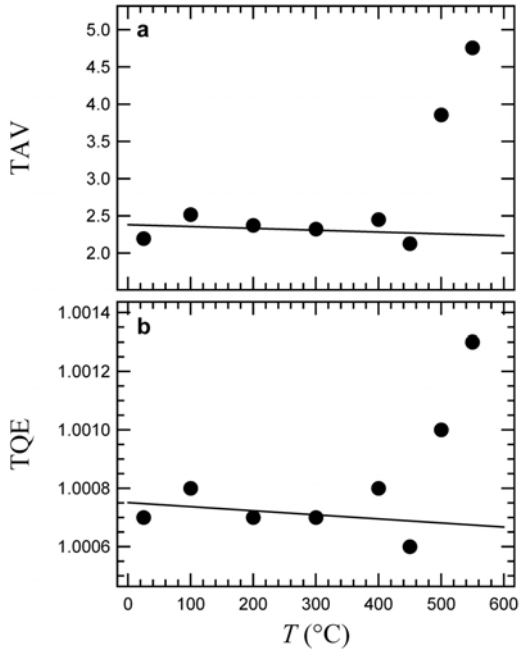

FIG. 5. Tetrahedral distortion parameters as a function of temperature. (*a*) Tetrahedral angle variance (TAV); (*b*) tetrahedral quadratic elongation (TQE). Linear regressions calculated in the range 25−450ºC are reported as solid lines.

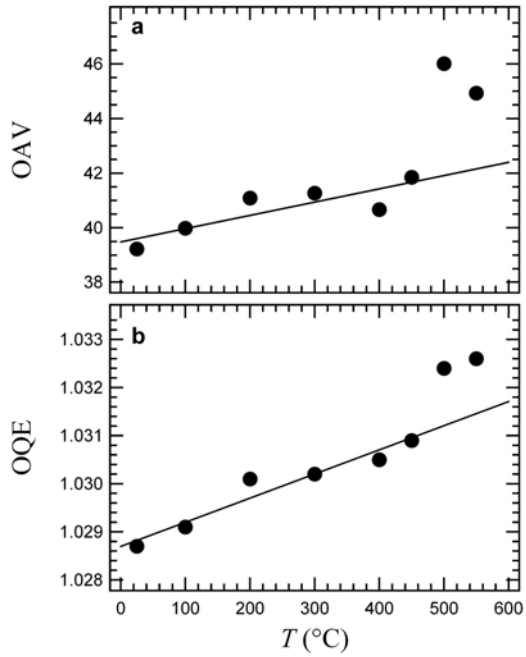

FIG. 6. Octahedral distortion parameters as a function of temperature. (*a*) Octahedral angle variance (TAV); (*b*) octahedral quadratic elongation (TQE). Linear regressions calculated in the range 25−450ºC are reported as solid lines.

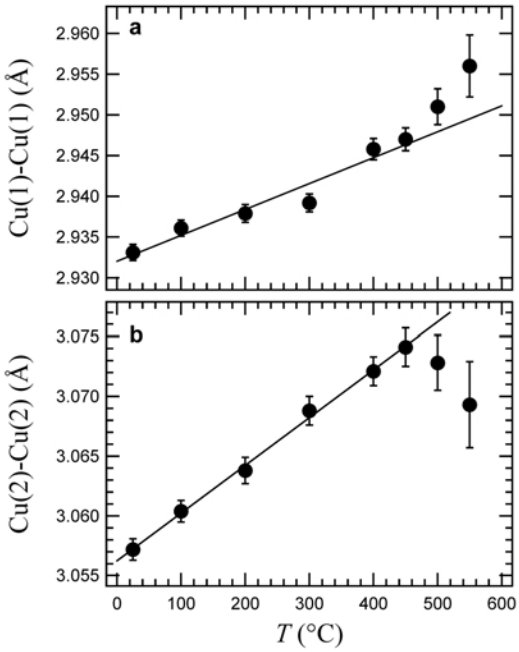

FIG. 7. Cation−cation distances as a function of temperature. (*a*) Cu(1)−Cu(1) distance along the chain; (*b*) Cu(2)−Cu(2) distance within the dimer.

(residual oxygen), hence the complete transformation can be written as:

$$2\ Cu_2(PO_4)(OH) \rightarrow Cu_4(PO_4)_2O + H_2O$$

Two hydroxyl groups belonging to an octahedron are then replaced by one oxygen atom and a molecule of H_2O is released. It is likely that the OH group that destabilizes must initially attract the H^+ from the adjacent OH group for condensation of the water molecule to be extracted. In Fig. 8*a*, it is evident that the O4−O4 (O4 is the H-bearing site) edge decreases sharply starting from 450ºC. As a consequence of this primary movement, the Cu(1)−O4 distances shorten while Cu(2)−O4 elongates, thus justifying the variations observed in the average Cu−O bond distances (see Fig. 4*a,b*). It is also worth noting that the apical Cu(1)−O bond distances do not elongate further at these temperatures, so to ensure proper coordination to the copper ion after one of the basal oxygen atoms is lost with dehydration. The PO_4 tetrahedron, even maintaining its polyhedral volume virtually unaltered, becomes much more distorted (see Figs 4*c*, 5) as oxygen atoms have to compensate for the drastic changes about to occur

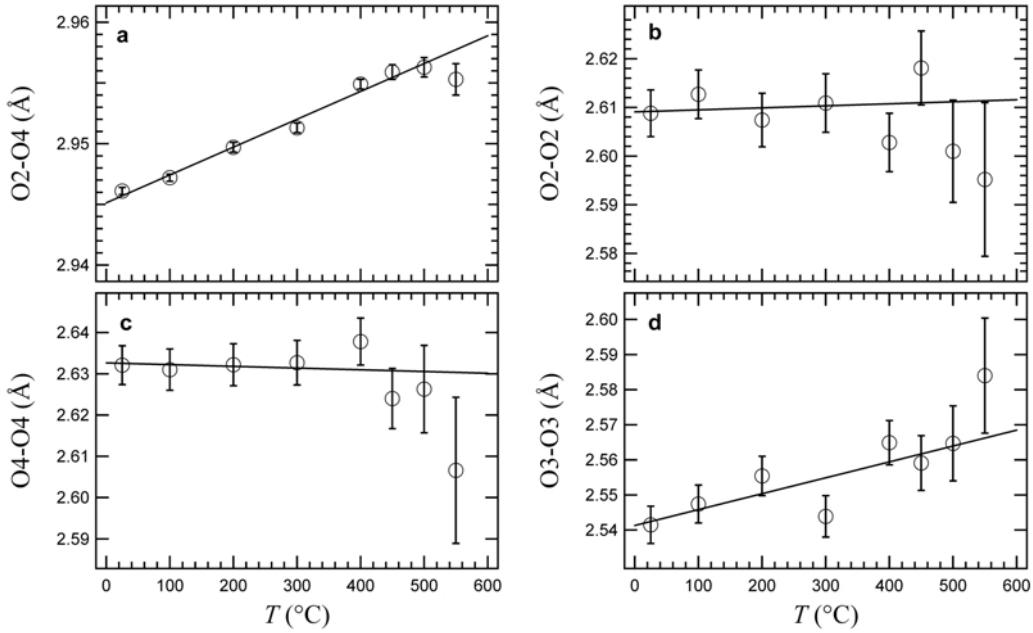

FIG. 8. Variation of selected polyhedral edges with temperature. (*a*) O2−O4, within each octahedron and indicative of the elongation of the chain; (*b*) O2−O2, shared by two octahedra along the chain; (*c*) O4−O4, shared by two octahedra along the chain and bearing the H atoms; (*d*) O3−O3, shared by two Cu(2) trigonal bipyramids. Linear regressions calculated in the range 25−450ºC are reported as solid lines.

in Cu environments. Such structural variations suggest an incipient transformation of libethenite $Cu_2(PO_4)(OH)$ into $Cu_4(PO_4)_2O$ by losing one water molecule.

Acknowledgements

The authors thank Dr E. Basso, Laboratorio Arvedi–CISRiC, University of Pavia, for the SEM/EDS analyses, and R. Gastoni, CNR-IGG, for preparing the sample. The authors also thank P. Ballirano and S.J. Mills for their comments.

References

Belik, A.A., Koo, H.-J., Whangbo, M.-H., Tsujii, N., Naumov, P. and Takayama-Muromachi, E. (2007) Magnetic properties of synthetic libethenite Cu_2PO_4OH: a new spin-gap system. *Inorganic Chemistry*, **46**, 8684–8689.

Blessing, R.H. (1995) An empirical correction for absorption anisotropy. *Acta Crystallographica*, **A51**, 33–38.

Blessing, R.H., Coppens, P. and Becker, P. (1974) Computer analysis of step-scanned X-ray data. *Journal of Applied Crystallography*, **7**, 488–492.

Brunel-Laügt, M., Durif, A. and Guitel, J.C. (1978) Structure cristalline de $Cu_4(PO_4)_2O$. *Journal of Solid State Chemistry*, **25**, 39–47.

Busing, W.R. and Levy, H.A. (1964) The effect of thermal motion on the estimation of bond lengths from diffraction measurements. *Acta Crystallographica*, **17**, 142–146.

Cordsen, A. (1978) A crystal-structure refinement of libethenite. *The Canadian Mineralogist*, **16**, 153–157.

Heritsch, H. (1940) Die Struktur des Libethenites $Cu_2(OH)[PO_4]$. *Zeitschrift für Kristallographie*, **102**, 1–12.

Huminicki, D.M.C. and Hawthorne, F.C. (2002) The crystal chemistry of phosphate minerals. Pp. 123–253 in: *Phosphates – Geochemical, Geobiological and Materials Importance* (M.L. Kohn, J. Rakovan and J.M. Hughes, editors). Mineralogical Society of America, Washington, D.C. and the Geochemical Society, St. Louis, Missouri, USA.

Ibers, J.A. and Hamilton, W.C. (1974) *International Tables for X-ray Crystallography*. Kynoch Press, Birmingham, UK, vol. 4, pp. 99–101.

Johnson, C.K. (1970*a*) Generalized treatments for thermal motion. Pp. 132–160 in: *Thermal Neutron Diffraction* (B.T.M. Willis, editor). Oxford University Press, Oxford, UK.

Johnson, C.K. (1970*b*) An introduction to thermal motion analysis. Pp. 220–226 in: *Crystallographic Computing* (F.R. Ahmed, editor). Munksgaard, Copenhagen.

Keller, P., Hess, H. and Zettler, F. (1979) Ladungsbilanzen an den verfeinerten Kristallstrukturen von Libethenit, Adamin und $Co[OH/AsO_4]$ und ihre Wasserstoffbrückenbindungen. *Neues Jahrbuch für Mineralogie, Abhandlungen*, **134**, 147–159.

Lehman, M.S. and Larsen, F.K. (1974) A method for location of the peaks in step-scan measured Bragg reflections. *Acta Crystallographica*, **A30**, 580–584.

Li, C., Yang, H. and Downs, R.T. (2008) Redetermination of olivenite from an untwinned single-crystal. *Acta Crystallographica*, **E64**, i60–i61.

Mills, S.J., Kampf, A.R., Poirier, G., Raudsepp, M. and Steele, I.A. (2010) Auriacusite, $Fe^{3+}Cu^{2+}AsO_4O$, the first M^{3+} member of the olivenite group, from the Black Pine mine, Montana, USA. *Mineralogy and Petrology*, **99**, 113–120.

North, A.C.T., Phillips, D.C. and Mathews, F.S. (1968) A semi-empirical method of absorption correction. *Acta Crystallographica*, **A24**, 351–359.

Robinson, K., Gibbs, G.V. and Ribbe, P.H. (1971) Quadratic elongation, a quantitative measure of distortion in co-ordination polyhedra. *Science*, **172**, 567–570.

Scheringer, C. (1972) A lattice dynamical treatment of the thermal motion bond-length correction. *Acta Crystallographica*, **A28**, 616–619.

Schneider, H. and Eberhard, E. (1990) Thermal expansion of mullite. *Journal of the American Ceramic Society*, **73**, 2073–2076.

Schwunck, H.-M., Moser, P. and Jung, W. (1998) The copper(II) oxide phosphate $Cu_4O(PO_4)_2$ in a new, orthorhombic modification by oxidation of a Tl/Cu/P alloy. *Zeitschrift für Anorganische und Allgemeine Chemie*, **624**, 1262–1266.

Sheldrick, G.M. (1998) *SHELX97 – Programs for Crystal Structure Analysis (Release 97-2)*. Institut für Anorganische Chemie der Universität, Göttingen, Germany.

Sheldrick, G.M. (2003) *SADABS*. University of Göttingen, Germany.

Xiao, F.-S., Sun, J., Meng, X., Yu, R., Yuan, H., Xu, J., Song, T., Jiang, D. and Xu, R. (2001) Synthesis and structure of copper hydroxyphospate and its high catalytic activity in hydroxylation of phenol by H_2O_2. *Journal of Catalysis*, **199**, 273–281.